Title

Extracting the average single-molecule biexciton photoluminescence lifetime from a solution of chromophores.

Journal

Optics Letters, 41(20)

ISSN

0146-9592

Authors

Bischof, Thomas S
Caram, Justin R
Beyler, Andrew P
et al.

Publication Date

2016-10-15

DOI

10.1364/ol.41.004823

Peer reviewed

Optics Letters

Extracting the average single-molecule biexciton photoluminescence lifetime from a solution of chromophores

THOMAS S. BISCHOF, JUSTIN R. CARAM, ANDREW P. BEYLER, AND MOUNGI G. BAWENDI*

Department of Chemistry, Massachusetts Institute of Technology, Cambridge, Massachusetts 02139, USA
**Corresponding author: mgb@mit.edu*

Received 14 July 2016; revised 29 August 2016; accepted 16 September 2016; posted 16 September 2016 (Doc. ID 270464); published 14 October 2016

We present a method for obtaining the average single-molecule biexciton lifetime from an ensemble of chromophores in solution. We apply this analysis to a series of core/shell CdSe/CdS quantum dot heterostructures with increasing shell thickness and find that the lifetime of the biexciton increases with increasing shell thickness, consistent with a simultaneous measurement of biexciton quantum yield.

OCIS codes: (030.5290) Photon statistics; (160.2540) Fluorescent and luminescent materials; (160.6000) Semiconductor materials.

http://dx.doi.org/10.1364/OL.41.004823

Colloidal quantum dots are used in applications requiring high optical flux and electrical charging, and the role of highly excited biexcitonic, trionic, and other multiexcitonic states is increasingly relevant to understanding performance-degrading phenomena such as blinking and photodarkening. This has led to increased interest in characterizing the statistics [1–4] and dynamics [3,5–10] of these states. Single-molecule methods provide detailed insight into the exact behavior of individual molecules, but they are labor-intensive and prone to selection bias. Ensemble lifetime-based methods are simpler to implement and provide averaged information, but these methods often require perturbative experimental conditions and statistical modeling to account for non-trivial photophysics [11–13].

The adaptation of single-molecule photon correlation methods to study ensembles of nanocrystals in solution enables the description of the average properties of individual chromophores, averaged over millions in solution [14–17]. For example, photon correlation Fourier spectroscopy (PCFS) can be used to study the average spectral dynamics of individual emitters [15,16,18–20]. We have also used second-order photon correlation ($g_0^{(2)}$) to measure the ensemble-averaged biexciton quantum yield ratio for a variety of materials, including CdSe, InP, and InAs [17]. These methods use intrinsic contrast between the single-molecule emission and that of the ensemble. This enables the isolation of the single-molecule contribution while operating under conditions of low excitation flux, decreasing the effects of blinking and photocharging [21,22]. These methods retain the power of the single-molecule interpretation while reporting average information about the ensemble, and are thus well-suited for screening new materials, which are not always sufficiently stable to withstand typical single-molecule spectroscopies [17].

Here we describe the measurement of the ensemble-averaged single-molecule biexciton lifetime, averaged for an ensemble of individual freely diffusing nanocrystals in solution. Our method is an extension of the photon-ordering concept described in Ref. [7], where photon pairs arising after a single excitation pulse are emitted from the biexciton and monoexciton, and can thus be identified by arrival order. We develop a method for measuring the Poissonian background present in an ensemble number-resolved experiment, which allows us to directly isolate the single-molecule contribution. We apply this method to a series of CdSe/CdS core/shell quantum dots with increasing shell thickness, and correlate the biexciton dynamics with the statistics obtained using solution $g_0^{(2)}$. The dataset for the shell series is same as the one used in Ref. [17].

In our experiment, a sample of quantum dots is excited using a pulsed laser source, and the photon arrival times are recorded as a triplet: the detection channel, the index of the excitation pulse, and the arrival time relative to that excitation pulse [Fig. 1(a)]. In a second-order correlation measurement ($g^{(2)}$), we calculate the difference in arrival pulse and arrival time for each pair of photons [illustrated in Fig. 1(b)], which encodes information about biexciton quantum yield, particle concentration, and diffusion rates [23]. Here we examine biexciton emission, which occurs with highest contrast in the "center" peak. In the single-molecule $g^{(2)}$ measurement, this center peak consists of pairs of photons arriving as a biexciton-monoexciton cascade, with some contribution from background emission or intrapulse re-excitation. In an ensemble measurement, the single-molecule signal sits on a Poissonian background resulting from emission by different nanocrystals. By comparing the long-time behavior of $g^{(2)}(\tau)$, for which the pairs of photons are increasingly likely to arise from distinct nanocrystals, with the center peak, we are able to distinguish these single-molecule and ensemble contributions.

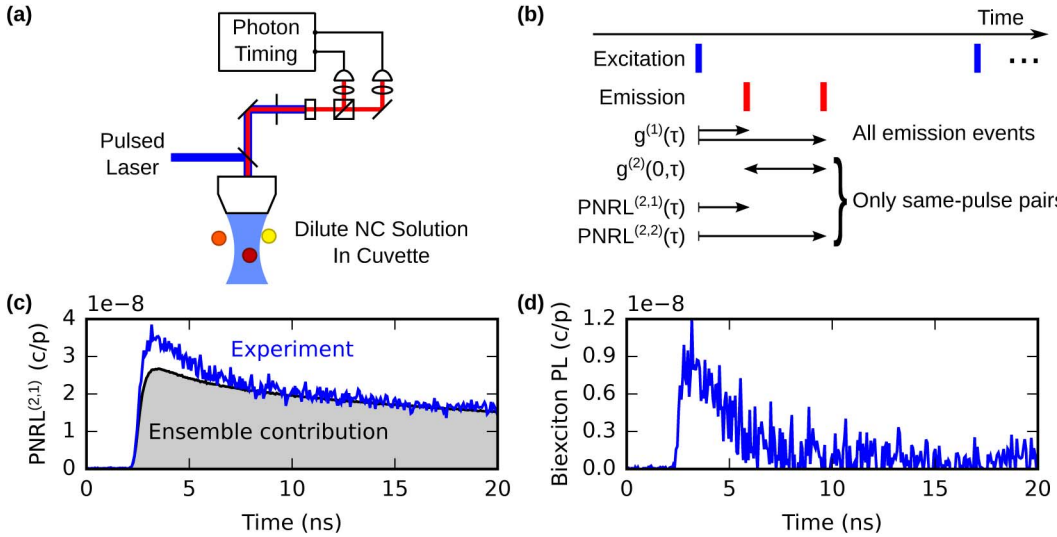

Fig. 1. (a) A schematic of the two-photon resolving microscope used in these experiments. (b) A depiction of the post-selection process. All photon events count toward the lifetime $g^{(1)}(\tau)$, but for pulses yielding multiple photons, we can perform a number-based post selection. For pulses yielding exactly two emission photons, we assign the first to $\mathrm{PNRL}^{(2,1)}(\tau)$ and the second to $\mathrm{PNRL}^{(2,2)}(\tau)$. The difference in the arrival times of the second and first photons counts toward $g^{(2)}(0,\tau)$, where the 0 indicates that the photons arrived after the same excitation pulse. (c) We use $g^{(1)}$ and Eq. (1) to measure the contribution of ensemble emission to two-photon events (gray), and compare this with the experimental result (blue). (d) The biexciton lifetime, averaged over all individual emitters in the solution, is the difference obtained between the experimentally measured $\mathrm{PNRL}^{(2,1)}(\tau)$ and the ensemble background [Eq. (4)].

In our analysis, any given excitation pulse can yield 0, 1, or 2 detected photons. The photon number-resolved lifetime (PNRL) is measured for a stream of photons by assigning photons to virtual detection channels according to the number and order of photons arriving after a given excitation pulse. Pairs of photons arriving after a single excitation pulse are assigned to $\mathrm{PNRL}^{(2,1)}(\tau)$ and $\mathrm{PNRL}^{(2,2)}(\tau)$, as the first and second photons to arrive, respectively. We only permit each physical detector to contribute a single photon per excitation pulse to suppress the effects of afterpulsing (this is effectively time gating at the repetition rate of the experiment). Because the biexciton photon is emitted before the monoexciton photon [7,8], this resolution of photon number and order isolates the biexciton contribution to $\mathrm{PNRL}^{(2,1)}(\tau)$ and the monoexciton contribution to $\mathrm{PNRL}^{(2,2)}(\tau)$.

This pair of signals results from four distinct types of events: emission of at least two photons from a single nanocrystal, emission from different nanocrystals, emission by a nanocrystal and some background source (e.g., dark counts), and emission from background sources. The latter three contribute to the "Poissonian" background observed in fluorescence correlation spectroscopy (FCS). As in other FCS methods [17,23], the magnitude of the background can be determined using the average photon detection rate. Here we use $g^{(1)}(\tau)$, which is the lifetime of all emission events on all detectors (excluding afterpulsing), normalized to the number of repetitions of the laser to yield the detection rate per unit time per excitation pulse.

The Poissonian background ($\mathrm{PNRL}_{\mathrm{bkg}}$) for $\mathrm{PNRL}^{(2,1)}(\tau)$ and $\mathrm{PNRL}^{(2,2)}(\tau)$ can be determined directly from the measured value of $g^{(1)}(\tau)$. In doing so, we must account for the effect of imposing time-ordering on emission events arising from largely independent sources, which causes $\mathrm{PNRL}^{(2,1)}(\tau)$ to decay faster than $g^{(1)}(\tau)$ and creates a slow rise in $\mathrm{PNRL}^{(2,2)}(\tau)$. Our analysis accounts for this effect, which is precisely determined using $g^{(1)}$ as follows:

$$\mathrm{PNRL}^{(2,1)}_{\mathrm{bkg}}(\tau) = \left(\frac{d-1}{d}\right) g^{(1)}(\tau) \left(\int_{\tau}^{T_{\mathrm{rep}}} g^{(1)}(t)\mathrm{d}t\right), \quad (1)$$

$$\mathrm{PNRL}^{(2,2)}_{\mathrm{bkg}}(\tau) = \left(\frac{d-1}{d}\right) \left(\int_{0}^{\tau} g^{(1)}(t)\mathrm{d}t\right) g^{(1)}(\tau), \quad (2)$$

where T_{rep} is the repetition time for the pulsed excitation source, and d is the number of detectors present in the system, which sets the geometric efficiency of the detection scheme (each detector may only report a single detection event per excitation pulse). The remaining expressions denote the joint probabilities of finding a photon at some time and another at some time before or after, respectively. We also measure $g^{(2)}(0,\tau)$, which is the difference in the arrival time between the second and first photons and is the center peak of a pulse-resolved $g^{(2)}$:

$$g^{(2)}_{\mathrm{bkg}}(0,\tau) = \left(\frac{d-1}{d}\right) \int_{0}^{T_{\mathrm{rep}}-\tau} g^{(1)}(t) g^{(1)}(t+\tau)\mathrm{d}\tau. \quad (3)$$

Here, the 0 in $g^{(2)}_{\mathrm{bkg}}(0,\tau)$ notes that the difference in the pulse index between the two photons is 0. For the first "side" peak, this would be 1.

The result of this analysis is shown in Fig. 1(c), where the gray-shaded curve represents the contribution of $\mathrm{PNRL}^{(2,1)}_{\mathrm{bkg}}$ to $\mathrm{PNRL}^{(2,1)}$, while the blue curve is the experimentally measured value. The difference between these two is the contribution of biexcitonic emission from individual molecules, averaged over the ensemble in solution [Fig. 1(d)]:

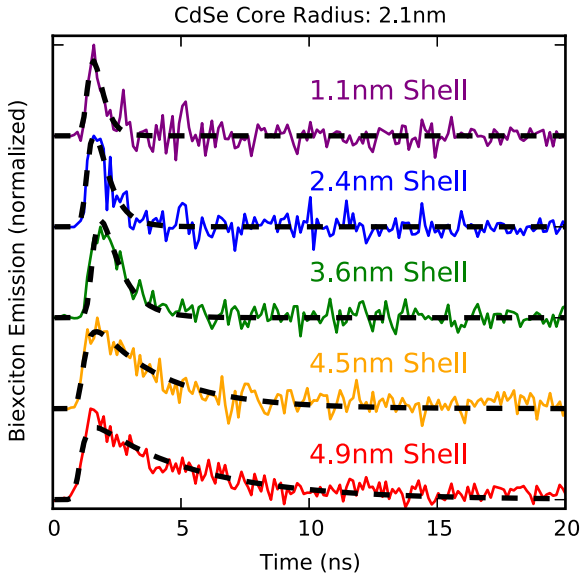

Fig. 2. Ensemble-averaged single-molecule biexciton lifetime for CdSe/CdS core/shell quantum dot samples grown from a single batch of CdSe particles, measured using $\mathrm{PNRL}^{(2,1)}$ with the Poissonian background removed. As the shell thickness increases, the lifetime of the emission increases. The dashed black curves are the best fit of a single exponential sample response. Time bins are 128 ps, and the curves are offset linearly.

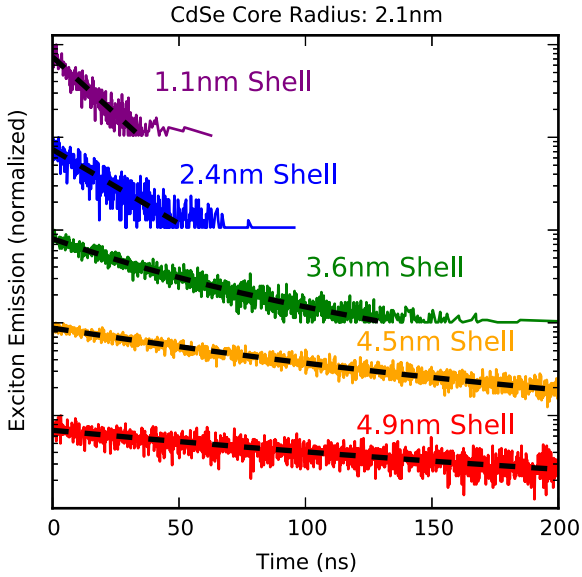

Fig. 3. Ensemble-averaged exciton lifetime for CdSe/CdS core/shell QD samples grown from a single batch of CdSe particles, measured using $g^{(2)}(0,\tau)$. As the shell thickness increases, the lifetime of the emission increases. The dashed black curves are the best fit of an exponential sample response. Time bins are 128 ps, and the curves are offset multiplicatively.

$$\mathrm{BX}(\tau) = \mathrm{PNRL}^{(2,1)}(\tau) - \mathrm{PNRL}^{(2,1)}_{\mathrm{bkg}}(\tau). \quad (4)$$

This method unambiguously resolves the biexciton dynamics of the nanocrystal: the signal presented in Fig. 1(d) can only arise from a state that permits emission of at least two photons. Our use of relatively low excitation flux ensures that this is the biexciton, as opposed to a higher-order multiexciton.

We now apply this method to characterize the effects of shell thickness on the biexciton in core/shell CdSe/CdS quantum dots. The biexciton emission quantum yield generally increases with the thickness of the CdS shell [17,24] or the introduction of a graded shell [3,4,25]. In Ref. [17], we examined the emission from a series of solutions of CdSe/CdS quantum dots with increasing shell thickness, grown from a single batch of core CdSe particles (2.1 nm radius). Applying Eq. (4) to this dataset, we obtain the biexciton emission shown in Fig. 2. The dashed black curves are the best fit for our sample response function (a single exponential convolved with the instrument response function, which is a Gaussian convolved with an exponential):

$$\mathrm{BX}(\tau) = [Ake^{-k\tau}] * [e^{-(\tau-\tau_0)/(2\sigma^2_{\mathrm{IRF}})} * \Theta(\tau)e^{-k_{\mathrm{IRF}}\tau}], \quad (5)$$

where Θ is the unit step function representing the arrival of the laser pulse. The parameters for the instrument response ($\sigma_{\mathrm{IRF}} = 0.14$ ns, $k_{\mathrm{IRF}} = 4.3$ ns^{-1}) are determined independently by measuring scattered light from the laser, and held constant during further fitting.

In order to relate this biexciton lifetime to the biexciton quantum yield, we must also have a measure of the exciton lifetime. For this we use $g^{(2)}(0,\tau)$ (Fig. 3), which primarily captures exciton emission, as opposed to $g^{(1)}(\tau)$, which is a mixture of all emissions. This is not a purely single-molecule signal: the relatively long emission lifetime reduces contrast between the single-molecule and ensemble response, preventing analysis akin to Eq. (4). We measure the exciton lifetime by fitting $g^{(2)}(0,\tau)$ with a single exponential response for the 1.1 and 2.4 nm samples, and with the sum of two exponentials for the other samples (the second exponential typically has a much longer lifetime and may be associated with electron traps [26]). We treat the shorter lifetime as the exciton radiative lifetime.

The lifetimes of the biexciton and exciton for each sample are reported in Table 1.

The biexciton in colloidal CdSe quantum dots is a bound pair of excitons, whose spin statistics dictate that the radiative lifetime is one quarter that of a single exciton [8]. The observed lifetime results from the combination of non-radiative processes (e.g., Auger recombination) with the intrinsic radiative rate, and thus we can measure the quantum yield of the biexciton through measurements of emission lifetime:

$$\mathrm{QY}_{\mathrm{BX}} = \frac{k_{\mathrm{BX,rad}}}{k_{\mathrm{BX}}} = \frac{4k_{X,\mathrm{rad}}}{k_{\mathrm{BX}}} = \frac{4\tau_{\mathrm{BX}}}{\tau_{X,\mathrm{rad}}}. \quad (6)$$

Table 1. Lifetime of the Biexciton and Exciton for Each Sample in the Shell Series, Obtained Using the Signals Shown in Figs. 2 and 3[a]

	Biexciton	Exciton Fit			
Shell (nm)	Lifetime (ns)	A_1	τ_1 (ns)	A_2	τ_2 (ns)
1.1	0.29(6)	—	17.6(1)	—	—
2.4	0.54(6)	—	27.1(3)	—	—
3.6	0.79(6)	0.31(3)	33(1)	0.69(2)	103(4)
4.5	2.7(2)	0.39(1)	82(1)	0.61(1)	341(5)
4.9	4.1(2)	0.27(1)	124(2)	0.73(1)	640(10)

[a]Values in parentheses are one standard deviation of error in the final digit obtained using the covariance matrix from functional fitting.

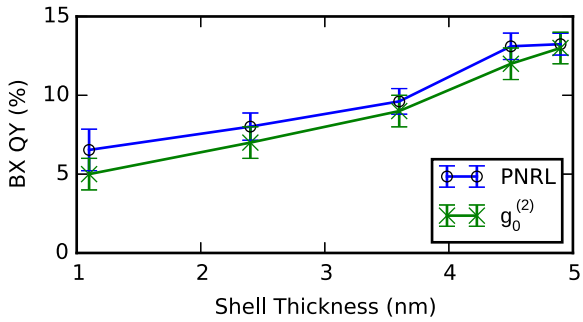

Fig. 4. Biexciton quantum yield for each sample, as determined by PNRL (blue °) or $g_0^{(2)}$ (green ×). For PNRL, the error bars are propagated from the fits for the biexciton and exciton dynamics, and for $g_0^{(2)}$, the error bars are determined by Poissonian statistics.

We assume that the experimentally measured exciton lifetime arises from the purely radiative state, for which emission occurs with quantum yield unity [5]. This assumption ignores the effects of photoluminescence intermittency ("blinking"), which may occur during continuous excitation. Blinking results in emissions arising from a mixture of states with various lifetimes and quantum yields [27], such that the measured lifetime typically underestimates the true exciton radiative lifetime and thus overestimates the biexciton quantum yield. In our experiment, we suppress the effects of these states by using low excitation flux and by permitting the nanocrystals to diffuse freely through the focal volume.

Applying the model in Eq. (6) to the data in Table 1 produces the blue curve of Fig. 4. This measurement simultaneously yields the statistical $g_0^{(2)}$ result, originally described in Ref. [17], in which we use the integrated area of $g^{(2)}(\tau)$ to determine the relative quantum yield of the biexciton and exciton, and it is shown as the green curve of Fig. 4. These dynamic and statistical methods produce estimates of biexciton quantum yield which are in good agreement, and so for this series of core/shell materials, the model of the biexciton as a bound pair of excitons is valid.

Our method to simultaneously characterize the statistics and dynamics of excitonic states in nanocrystals can be applied to other material systems. For example, the development of core/shell materials with gradient shell interfaces permits engineering of the multiexcitonic dynamics and statistics [3,4]. Application of PNRL to these materials would enable the rapid screening of entire synthetic batches, bypassing the need for labor-intensive single-molecule methods, removing user selection bias, and permitting the examination of new materials which are not yet suitable for detailed single-molecule study.

In this Letter, we demonstrate a photon correlation method for the resolution of the ensemble-averaged single-molecule biexciton lifetime from a solution-based photoluminescence measurement. We use the method to study emission from a series of CdSe/CdS core/shell quantum dots and find that the biexciton lifetime increases monotonically with increasing shell thickness. The biexciton quantum yield as measured by this dynamical method is consistent with the statistical solution $g_0^{(2)}$ method.

Funding. U.S. Department of Energy (DOE) (DE-SC0001088, DE-FG02-07ER46454); Office of Science (SC); Basic Energy Sciences (BES).

Acknowledgment. T. S. B. thanks Mark W. B. Wilson for many helpful discussions. The authors acknowledge the other authors of [17], whose work produced the CdSe/CdS dataset studied in this Letter. The full dataset and the software used for analysis are available upon request.

REFERENCES

1. G. Nair, J. Zhao, and M. G. Bawendi, Nano Lett. **11**, 1136 (2011).
2. Y. S. Park, A. V. Malko, J. Vela, Y. Chen, Y. Ghosh, F. García-Santamaría, J. A. Hollingsworth, V. I. Klimov, and H. Htoon, Phys. Rev. Lett. **106**, 187401 (2011).
3. Y. S. Park, W. K. Bae, L. A. Padilha, J. M. Pietryga, and V. I. Klimov, Nano Lett. **14**, 396 (2014).
4. M. Nasilowski, P. Spinicelli, G. Patriarche, and B. Dubertret, Nano Lett. **15**, 3953 (2015).
5. B. Fisher, J. M. Caruge, D. Zehnder, and M. Bawendi, Phys. Rev. Lett. **94**, 087403 (2005).
6. F. García-Santamaría, S. Brovelli, R. Viswanatha, J. A. Hollingsworth, H. Htoon, S. A. Crooker, and V. I. Klimov, Nano Lett. **11**, 687 (2011).
7. D. Canneson, I. Mallek-Zouari, S. Buil, X. Quélin, C. Javaux, B. Dubertret, and J. P. Hermier, New J. Phys. **14**, 063035 (2012).
8. D. Canneson, L. Biadala, S. Buil, X. Quélin, C. Javaux, B. Dubertret, and J. P. Hermier, Phys. Rev. B **89**, 035303 (2014).
9. Y. S. Park, W. K. Bae, J. M. Pietryga, and V. I. Klimov, ACS Nano **8**, 7288 (2014).
10. N. S. Makarov, S. Guo, O. Isaienko, W. Liu, I. Robel, and V. I. Klimov, Nano Lett. **16**, 2349 (2016).
11. G. Nair, S. M. Geyer, L. Y. Chang, and M. G. Bawendi, Phys. Rev. B **78**, 125325 (2008).
12. V. I. Klimov, J. A. McGuire, R. D. Schaller, and V. I. Rupasov, Phys. Rev. B **77**, 195324 (2008).
13. F. T. Rabouw, M. Kamp, R. J. A. van Dijk-Moes, D. R. Gamelin, A. F. Koenderink, A. Meijerink, and D. Vanmaekelbergh, Nano Lett. **15**, 7718 (2015).
14. A. V. Orden and J. Jung, Biopolymers **89**, 1 (2008).
15. L. F. Marshall, J. Cui, X. Brokmann, and M. Bawendi, Phys. Rev. Lett. **105**, 053005 (2010).
16. J. Cui, A. P. Beyler, L. F. Marshall, O. Chen, D. K. Harris, D. D. Wanger, X. Brokmann, and M. G. Bawendi, Nat. Chem. **5**, 602 (2013).
17. A. P. Beyler, T. S. Bischof, J. Cui, I. Coropceanu, D. K. Harris, and M. G. Bawendi, Nano Lett. **14**, 6792 (2014).
18. L. Coolen, X. Brokmann, P. Spinicelli, and J. P. Hermier, Phys. Rev. Lett. **100**, 027403 (2008).
19. L. Coolen, P. Spinicelli, and J. P. Hermier, J. Opt. Soc. Am. B **26**, 1463 (2009).
20. J. Wolters, N. Sadzak, A. W. Schell, T. Schröder, and O. Benson, Phys. Rev. Lett. **110**, 027401 (2013).
21. G. Nair and M. G. Bawendi, Phys. Rev. B **76**, 081304 (2007).
22. J. A. McGuire, J. Joo, J. M. Pietryga, R. D. Schaller, and V. I. Klimov, Acc. Chem. Res. **41**, 1810 (2008).
23. J. Cui, A. P. Beyler, T. S. Bischof, M. W. B. Wilson, and M. G. Bawendi, Chem. Soc. Rev. **43**, 1287 (2014).
24. B. D. Mangum, S. Sampat, Y. Ghosh, J. A. Hollingsworth, H. Htoon, and A. V. Malko, Nanoscale **6**, 3712 (2014).
25. R. Vaxenburg, A. Rodina, E. Lifshitz, and A. L. Efros, Nano Lett. **16**, 2503 (2016).
26. Y. Gao and X. Peng, J. Am. Chem. Soc. **137**, 4230 (2015).
27. A. I. Chizhik, I. Gregor, and J. Enderlein, Nano Lett. **13**, 1348 (2013).